

A NOVEL METHOD FOR DISCERNING THE CONTRIBUTIONS OF SHALLOW AND DEEP CONVECTION IN THE EVOLUTION OF TROPICAL CYCLONES IN MODEL SIMULATIONS, WITH IMPLICATIONS FOR USE WITH SATELLITE OBSERVATIONS

5B.6

Daneisha S. Blair^{1,*}, Guosheng Liu¹, Svetla Hristova-Veleva², Ziad Haddad², Sai Prasanth²

¹ Florida State University, Tallahassee, FL

² Jet Propulsion Laboratory, California Institute of Technology, Pasadena, CA

1. INTRODUCTION

Convective storms and tropical convective systems in particular produce much of the Earth's rainfall and are responsible for the bulk of the mass, heat and moisture transport from the Earth's surface into the upper troposphere. What makes convective storms develop and grow the way they do? Our understanding of these processes is still lacking, hampering our ability to properly represent these processes in numerical weather prediction models (Zhang, et al., 2013; Dai, et al., 2022; Liu, et al., 2022). NASA's 2018 Earth Sciences decadal survey highlighted several scientific questions whose resolution using satellite observations should receive the highest priority in the coming decade. These include the problem of improving our understanding and modeling of convective storms, and proper evaluation of their feedback on the environment and on the Earth System as a whole. Of particular importance in that regard is understanding when and how deep convection develops and how it aggregates and organizes spatially is crucial for comprehending convective storm development, especially in tropical cyclone (TC). While deep convection's pivotal role is acknowledged, it cannot be identified from satellite observation today. Thus, the question persists: how can deep convection be effectively detected from space?

Since the interaction of rain and wind is fundamental to the existence of convective systems, the investigations to answer this question will have to improve our understanding of how the interaction between small-scale (vortex- and convective-scale) features such as vertical profiles of wind divergence relate to the characteristics of the vertical transport in deep convective updrafts and the development of precipitation. Deep convection is a critical component of TCs that plays a crucial role in the development, intensity, and evolution of a TC (Liu, et al., 2022; Zhang, et al., 2022). The objective of this study is to develop a robust relationship between the vertical velocity and the observables precipitation and near-surface wind divergence using geophysical variables that are readily available in model simulations.

* *Corresponding author address:* Daneisha S. Blair, Florida State University, Tallahassee, FL; email:db18g@fsu.edu.

The connection between near-surface divergence and vertical transport has long been touted as essential to understanding the process of moist convection but has never been objectively quantified. The role of these small-scale processes on deep convection in TC is less well known than that of large-scale (environmental-scale) factors such as sea surface temperature (SST), atmospheric moisture, and vertical wind shear (VWS) (Gray, 1968; Merrill, 1988; DeMaria & Kaplan, 1994a; Kaplan & DeMaria, 2003; Leighton, et al., 2018). Much research over the past decades has focused on identifying small-scale (vortex- and convective-scale) properties and their impact on TC intensification.

Processes that occur on the vortex-scale such as radial inflow in the lower troposphere, particularly in the planetary boundary layer (PBL), can establish regions of enhanced convergence which have been shown to be preferred regions for the initiation of convection (Rogers, et al., 2013; Rogers, et al., 2015; Miyamoto & Takemi, 2015). PBL radial inflow impacts on TC intensification have been studied by Montgomery et al. (2014), Sanger et al. (2014), Montgomery & Smith (2012), and Smith et al. (2009). In their work, they discuss two modes of radial inflow: a deep, relatively weak inflow that converges absolute angular momentum above the boundary layer, where it is conserved; and a strong inflow in the lowest 1 km that also converges angular momentum and creates supergradient flow as the inflowing air converges absolute angular momentum at a rate that exceeds its dissipation to the ocean surface via friction, providing one possible forcing mechanism for deep convection.

Broadly speaking, there have been two avenues of research exploring TC intensification. In the first, the focus has been on the processes that occur on the convective-scale. Several airborne, modeling, and other satellite-based studies have observed intermittent occurrence of deep, strong convective bursts within the inner core when TCs undergo intensification (i.e., Kelley, et al., 2004; Hendricks, et al., 2004; Braun, 2006; Montgomery, et al., 2006; Reasor, et al., 2009; Guimond, et al., 2010; Rogers, et al., 2013; Rogers, et al., 2015; Stevenson, et al., 2014; Susca-Lopata, et al., 2015). Alternatively, the focus has been on the observable, larger-scale, azimuthally symmetric convection during TC intensification. Several satellite-based studies i.e., Jiang, (2012); Kieper & Jiang, (2012); Zagrodnik & Jiang,

(2014); Tao & Jiang, (2015) have noted that it is primarily the azimuthal coverage of shallow and moderate convection, indicated by a ring of precipitation in 37-GHz microwave images that highlights rainfall and weak-to-moderate updrafts, that distinguishes TCs about to undergo significant intensification (indicator of RI). This occurs when the ring is at least 90% closed and dominated by shallow warm precipitation extending from near the freezing level to the surface. See Fig. 1 for an illustration of the concepts. The relative importance of deep versus moderate/shallow convection in TC intensification and RI is an area of debate, and research is ongoing to address it. Another very important aspect of the TC intensification process is regarding the location of the convective activity with respect to vortex structure as depicted by the radius of maximum wind (RMW). Rogers et al. (2013) found that for intensifying hurricanes, the peak in the distribution of deep convective bursts (CBs) was preferentially located inside the RMW, whereas for steady-state hurricanes the CBs were primarily located outside the RMW. Such a difference in the radial distribution of CBs was deemed important based on the balance arguments invoked Shapiro & Willoughby (1982), Schubert & Hack (1982), Nolan et al. (2007), and Vigh & Schubert (2009). They emphasized that the response of a vortex to diabatic heating depends on the efficiency of the heating which is maximized when it takes place within the RMW. Despite progress, detailed understanding processes on deep convection is still lacking and needs much room for improvement. Indeed, this gap in our knowledge has fueled the objective of this paper viz. to contribute in a most direct way, through the development of an observations-based (satellite-like) proxy-detector of mature, deep convection within TCs.

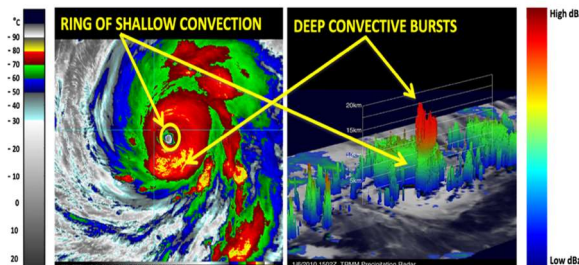


Figure 1. Structure of precipitation as revealed by IR images (left) and TRMM 3-dimensional (3D) radar reflectivity (right). Illustrated are the deep localized convection and the shallow, more symmetric one.

2. DATA

This study utilizes output data from three WRF Single-Moment Microphysics Scheme (WSM6) experiments simulating 2005's category-5 Hurricane Rita conducted by Hristova-Veleva et al. (2021). Their work highlighted that storms with very similar locations, intensity, and speed can have very different convective structures. Our aim here is to select from an ensemble of

simulations of Hurricane Rita, focusing on members with different convective organizational structures over the course of the TC's intensification, with the ultimate goal of developing a robust relationship between the vertical velocity and the observables precipitation and near-surface wind divergence. The primary aim of the Hristova-Veleva et al. (2021) study was to analyze the comparison between observed and forward simulated radiometric signatures of precipitation to determine what particle size distribution (PSD) assumptions result in the most realistic simulated hurricanes. Therefore, we examine the output data from the simulated 2005's category-5 Hurricane Rita for sensitivity experiments (S2, S5, and S7) from Hristova-Veleva et al. (2021) study.

The WRF modeling system has been designed to study mesoscale and convective scale processes and to provide an advanced mesoscale forecast and data assimilation system for broad use in both research and operations (Klemp, 2006). Moreover, the model allows us to examine all of the related variables in the atmospheric boundary layer, albeit within the constraints of the model parameterization. The WRF simulations began with initial conditions provided by Geophysical Fluid Dynamics Laboratory (GFDL) model analysis, valid on 19 September 2005 at 18:00Z. The model has a spatial resolution of 1.3 km, covering ~ 500 x 500 km with a temporal resolution of 30 minutes for experiment (S2) and 60 minutes for experiments (S5) and (S7). The fine spatial and temporal resolution of the model allows us to analyze the mesoscale convective activities such as precipitation, vertical velocity, and wind divergence and their response to the time evolution of TC intensity change. The model atmospheric vertical layer is ~20 km deep, which will give us the advantage of examining lower-level and upper-level divergence with respect to maximum updraft and precipitation.

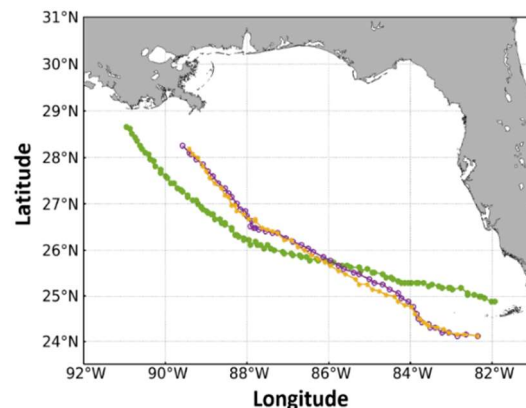


Figure 2. Plots of WRF-simulated track of Hurricane Rita for experiments S2 (green), S5 (purple), and S7 (orange) at 30-min intervals from 0000 UTC 21 Sept. to 0230 UTC 23 Sept. 2005 for S2 and 1-h intervals from 2200 UTC 20 Sept. to 0200 UTC 23 Sept. 2005 for S5 and S7.

3. METHOD

As stated earlier, our goal is to develop a robust relationship between the vertical velocity and the observables precipitation and near-surface wind divergence, we focus on the following variables of interest that are readily available in model simulations: (i) Precipitation: our results are focused on the use of the total column condensate (TCC). (ii) Vertical velocity: our results are focused on the use of maximum vertical velocity in a column. (ii) Wind divergence: the wind divergence computation adapts the work Holbach & Bourassa (2014).

We began addressing our goal by analyzing point-wise correlation between surface divergence and maximum vertical velocity in each column of a single scene at 0000 UTC 22 Sept. 2005 from the experiment (S2) of the model simulation of Hurricane Rita. Fig. 3 illustrates the variables that we first considered: the divergence of the surface winds and the maximum vertical velocity in each column. Addressing our goal of establishing a relationship between surface wind divergence and vertical velocity, we investigated the joint distribution of the two. However, interestingly, the point-wise distributions showed no such correlation or exploitable relationships (Fig. 3c).

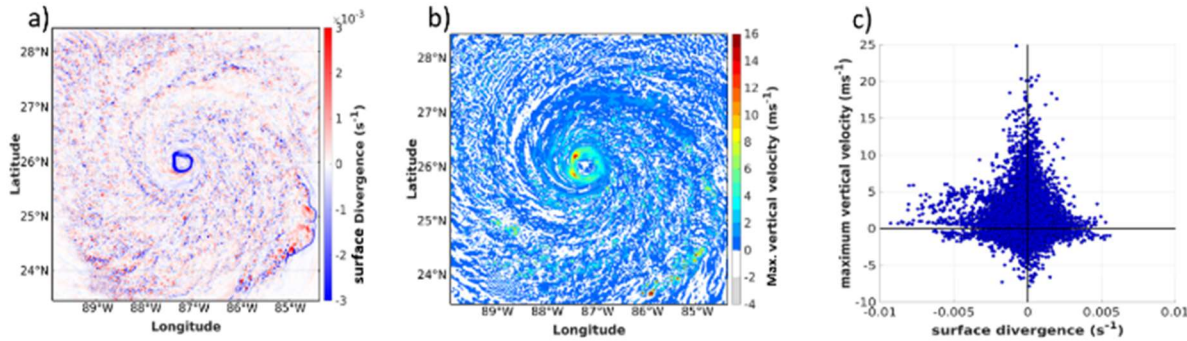


Figure 3. Structure of experiment (S2) WRF-simulated hurricane Rita at 00 UTC 22 Sept. 2005 for a) 10m-surface winds divergence, b) maximum vertical velocity in each column, and c) scatterplot of maximum vertical RESULTS

Why does this point-wise correlation show no correlation between the two variables? One possible explanation is the non-vertical orientation of updrafts within storms, especially in severe thunderstorms or tropical cyclones. The slanting of updrafts within a storm is a result of intricate interplays between factors such as wind shear, atmospheric stability, and the storm's internal dynamics (Pendergrass & Willoughby, 2009; Hazelton, et al., 2015). Consequently, a suitable approach is to correlate maximum vertical velocity within a column with integrated layers of wind divergence at various altitudes.

In this study, we investigated joint distributions of a few integral descriptions of near-surface wind divergence and a few representative descriptions of maximum vertical velocity within a column, as presented in Table 2. The goal here is to capture the physically important features of the dynamics of storm flow. This entails analyzing the divergence fields across low-level, mid-level, and upper-level atmospheric layers, along with varying intensities of maximum updraft within a column as indicators of the convective updraft's strength.

Wind divergence (X)	Maximum vertical velocity (Y)
D1 (divergence integrated from 0-3 km)	W1 (3x3 max. vertical velocity within a column > 0.5 m/s)
D2 (divergence integrated from 3-6 km)	W2 (3x3 max. vertical velocity within a column > 1 m/s)
D3 (divergence integrated above 6 km)	W3 (3x3 max. vertical velocity within a column >2 m/s)
D4 (3x3 divergence integrated from 0-3 km)	W4 (5x5 max. vertical velocity within a column > 0.5 m/s)
D5 (3x3 divergence integrated from 3-6 km)	W5 (5x5 max. vertical velocity within a column > 1 m/s)
D6 (3x3 divergence integrated above 6 km)	W6 (5x5 max. vertical velocity within a column >2 m/s)

Table 2. X column shows vertically-averaged divergence fields between 0-3 km (D1), 3-6 km (D2), >6 km (D3) and the same as D1, D2, and D3 but, then horizontally-smoothed (3x3 km averaged) for D4, D5, and D6. Y column shows the column maximum vertical velocity that is filtered for values greater than 0.5 ms⁻¹ (W1), 1 ms⁻¹ (W2), 2 ms⁻¹ (W3) then horizontally-smoothed (3x3 km averaged) and the same as W1, W2, W3 but, then horizontally-smoothed (5x5 km averaged) for W4, W5, and W6.

Next, we used canonical correlation analysis (CCA) to extract the importance between the descriptors of the divergence variables and the vertical velocity variables. CCA is a statistical technique used to analyze the relationships between two sets of variables. It determines

what linear combinations maximize the correlation between two scalar quantities (Hotelling, 1992).

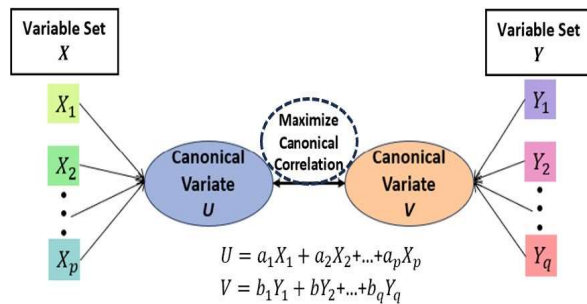


Figure 4. Schematic illustration of canonical correlation analysis. The objective is to find a linear combination of variable sets X and Y by maximizing the linear correlation between the two sets of new canonical variables U and V.

As a result, in this study, we obtained six pairs of canonical variables (U1-U6 for the divergence; V1-V6 for the vertical velocity) that capture the correlations, in a descending order of significance, with the U1/V1 correlations being of the highest significance. Fig. 5a illustrates the U1/V1 correlations, showing a remarkable improvement as compared to Fig. 3c. Analyzing the relative weight of the different contributors, we realized that the most important divergence contributor appeared to be that of the upper-level divergence. Indeed, this is to be expected, signifying that strong updrafts would have high upper-level divergence (a manifestation of the continuity equation).

To dig deeper into the unknown, we excluded the predictable variables, removing upper-level wind divergence fields D3 and D6, as well as maximum vertical velocity fields W2, W3, and W6. W2 was excluded due to its smaller spatial extent compared to W5, which offers better coverage for analyzing updraft characteristics, particularly given the non-vertical orientation of updraft fields. Furthermore, we excluded vertical velocity fields W3 and W6 based on the relative weight of each of the variables. This result obtained four pairs of vector variables (U1-U4) for the wind divergence and three pairs of vector variables (V1-V3) for the vertical velocity. Fig. 5b shows the highest significance correlation U1/V1 of this analysis, which shows a very interesting result of two-pronged nature of the correlations. We separate the two prongs of the correlations in Fig. 5b into experiments for $U1 \geq V1$ versus $U1 \leq V1$ and examine the insights that can be gained.

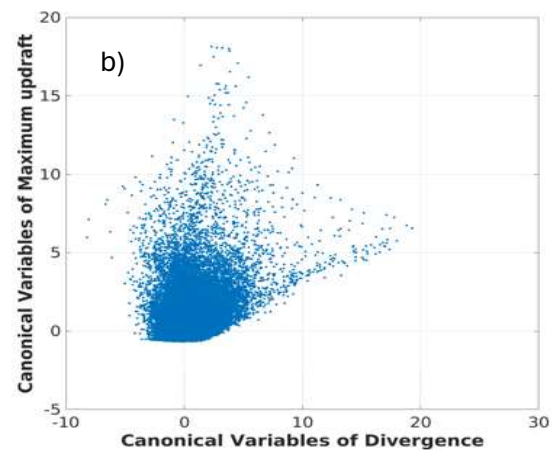
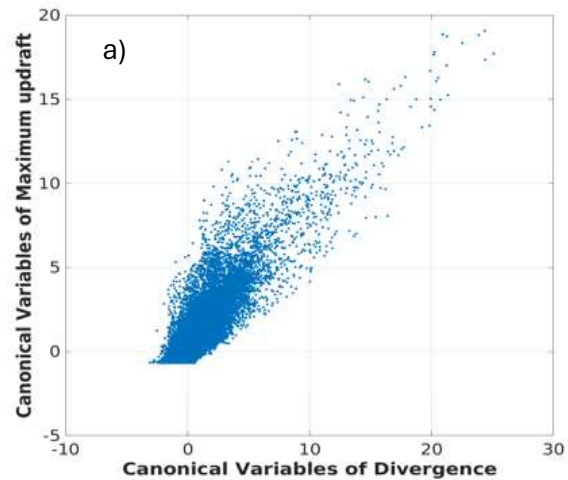


Figure 5. a) shows the first canonical correlation result of the first column and the second column in table 2 (i.e. U1 vs V1) and b) As in a) except for after excluding some of the descriptive parameters.

Fig. 5 illustrates the insights that can be gained from examining separately each of the two prongs of the correlations in Fig. 5b – i.e. **separating the cases for $U1 \geq V1$ versus $U1 \leq V1$** . Fig. 6a shows the horizontally-smoothed (3x3 km averaged) divergence, then vertically-averaged in the lowest level (0-3 km). An intricate interplay of divergence/convergence patterns is revealed. But what does this mean? Figs. 6b and 6c show the same field, but now for each of the two prongs/masks ($U1 \geq V1$ and $U1 \leq V1$). A remarkable separation is revealed with **$U1 \geq V1$ depicting low-level convergence and $U1 \leq V1$ regime depicting low-level divergence**. But what do these two regimes tell us? Relating one of the divergence measures (D4 from Table 2) to one of the measures of maximum vertical velocity (W1) for all points that satisfy the condition $U1 \geq V1$ now reveals a strong relationship (Fig. 6d). Comparing Figs. 6d and 3c show a dramatic improvement in the correlations, revealing how much information our analysis approach has revealed.

The point-wise distributions now revealed a strong relationship, which indeed shows as expected that on average low-level convergence relates to the updraft.

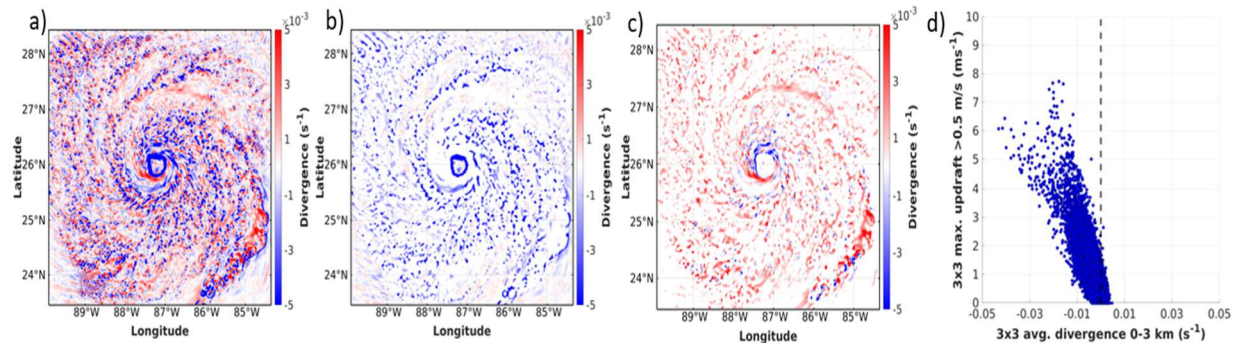


Figure 6. Structure of a) D4 from Table 2 (the 3x3 averaged divergence integrated between 0 – 3 km), b) pronged correlation of regime $U1 \geq V1$ from Fig. 5b, c) pronged correlation of regime $U1 \leq V1$ from Fig. 5b, and d) scatterplot of D4 vs W1 (from Table 2) for data points of regime $U1 \geq V1$ for WRF-simulated hurricane Rita of experiment (S2) at 00 UTC 22 Sept.

The above analyses revealed the importance of properly separating the two regimes – the low-level divergence and the low-level convergence. Here, we investigated how each of them is related to the vertically-integrated condensate. We wanted to see whether the regimes separate further, depending on the amount of the TCC. After analyzing the PDF of the TCC, we decided to define two precipitation regimes: TCC between $<2 \text{ kgm}^{-2}$ and TCC $>2 \text{ kgm}^{-2}$ resulting in the development of four different groups.

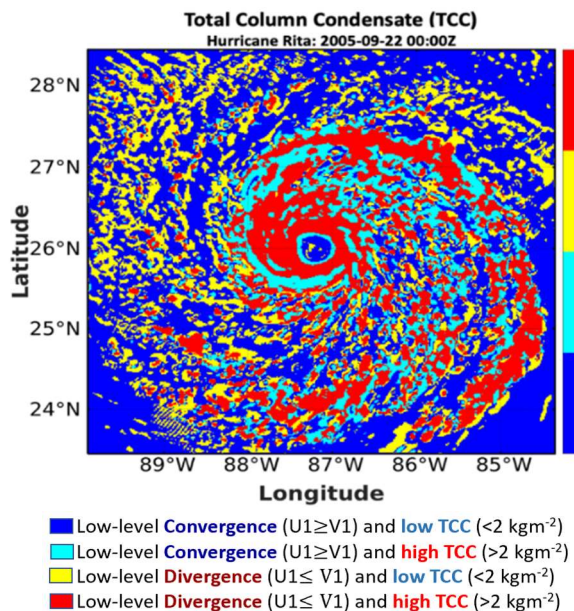


Figure 7. Spatial distribution of the four regions as defined by the low-level divergence/convergence, maximum updraft, and the TCC for WRF-simulated hurricane Rita of the experiment (S2) at 00 UTC 22 Sept.

Fig. 7 shows the spatial distribution of the four different groups as defined by the low-level wind divergence/convergence, maximum updraft, and TCC. It is very interesting to observe the very coherent structures of each of the 4 groups and the interplay between them. For example, the inner eyewall is occupied by a region of low-level convergence and low TCC values. This is immediately surrounded by a region of low-level divergence and high TCC values, possibly representing the mature convection in the hurricane eyewall.

What convective structures do the four regimes represent? To uncover this, we computed, separately for each of the four regions, the mean vertical profiles of wind divergence, vertical velocity, and condensate water content (CWC). Fig. 8 shows the mean vertical profiles for each of the four regions. It is remarkable to note that each of these four groups represents a very well-known class of convective precipitation structures (modes of precipitating structures) as described from left to right: mostly clear air (**dark blue**); developing convection (**cyan**); stratiform precipitation (**yellow**); mature convection (**red**).

In Fig. 8, the low-level convergence and low TCC values (**the dark-blue regime**) appear to represent the clearest atmosphere surrounding the storm, with general near-surface convergence (typical for a hurricane environment), very weak vertical velocity, and very low intensity condensation. Indeed, the region with low-level convergence but high TCC (**the cyan regime**) represents the typical profiles of shallow (developing) convection – strong near-surface convergence, vertical velocity, and total condensate that are bottom-heavy (have their peak in the lower troposphere, below 5 km in altitude, representing mostly warm-rain processes). This region is also observed to be in the immediate vicinity of the red region. The region with low-level divergence and high TCC values (**the red regime**) represents the region of

mature convection in which the vertical velocity is strong and top-heavy (with a broad peak at the middle and the upper troposphere). This is accompanied by a precipitation structure that now shows more elevated precipitation (i.e. twice as much condensate at 6 km as compared to the region of shallow convection). Another important characteristic of the mature convection is the strong near- surface divergence, to be expected in relation to low-level downdrafts under the mature convection that is contributing to the development of the cold pools. In that sense, the fact that the shallow (developing) convection (**the cyan regime**) is found in the immediate vicinity of the mature one is to be expected, considering that new convection develops at the leading edges of the diverging cold pools as conceptually illustrated in Fig. 9. The region with low-level divergence and low TCC values (**the yellow regime**) represents a very important category of precipitating structures. These vertical profiles are very typical of stratiform precipitation, showing near-surface divergence, associated with generally weak precipitation throughout the column, and with a very distinct profile of the vertical velocity that features upper-level rising (in the portion above the melting level) on top of low-level mesoscale downdrafts that are characteristic of the stratiform regions and are the manifestation of the evaporatively-induced sinking that results from the entrainment of dry midlevel air into the regions of the stratiform clouds.

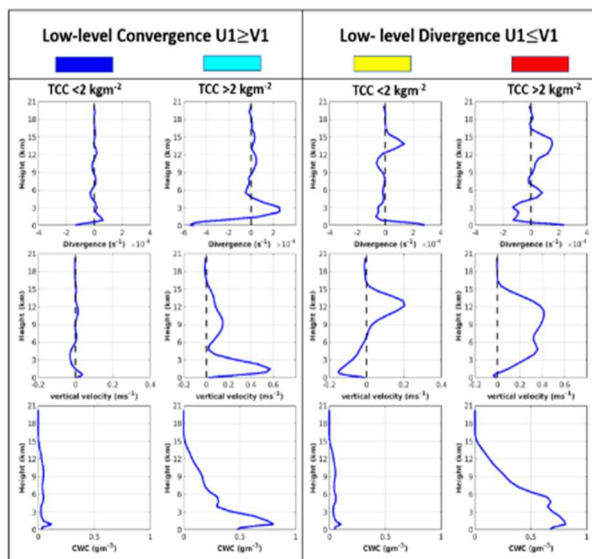


Figure 8. Mean vertical profiles of: divergence (top row), vertical velocity (middle row), and condensate water content (bottom row). These vertical profiles were computed separately over each of the four regions of interest: Low-level convergence (the left two columns, with the TCC $< 2 \text{ kgm}^{-2}$ on the left and the TCC $> 2 \text{ kgm}^{-2}$ on the right) and the same separation by TCC values but for the cases of low-level divergence (the right two columns). The color legend for the spatial distribution in

Fig. 7 is shown at the top of each column. Note that each of the four regions shows a distinct set of profiles that clearly describe one of the well-known modes of precipitating structures as described from left to right: mostly clear air (dark blue); shallow (developing convection) (cyan); stratiform precipitation (yellow); deep convection (red).

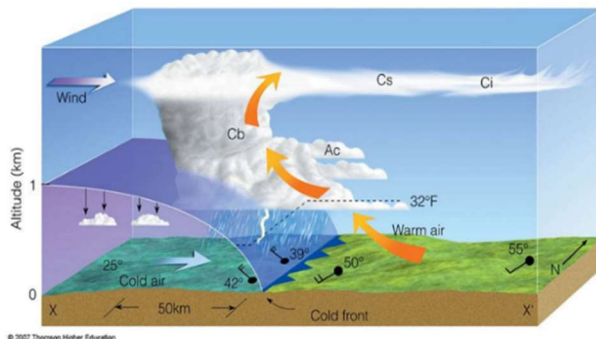


Figure 9. A schematic of the interactions between the mature convection, the cold pool beneath, and the convergence it generates on its leading edge that forces, through convergence with the environmental air, the development of new convection.

Subsequently, we applied the same methodology to examine the correlation between column-maximum vertical velocity, near-surface divergence, and total column condensate (precipitation) across all the timesteps for experiments (S2), (S5), and (S7). Figs. 10-12 show the mean and ± 1 standard deviations vertical profiles of wind divergence, vertical velocity, and CWC for each of the four convective groups across all timesteps of the WRF-simulated hurricane Rita for each experiment. It is indeed encouraging to observe that our methodology for establishing a correlation between vertical velocity and the observables near-surface divergence and total condensate can develop a classification of four convective regions. Each of these regions exhibits characteristic vertical structures representing the following categories: clear air in the storm environment, developing shallow convection, stratiform convection, and deep (mature) convection. This classification remains robust across varying simulations of Hurricane Rita's structure, intensity, and evolution.

(a) Experiment (S2)

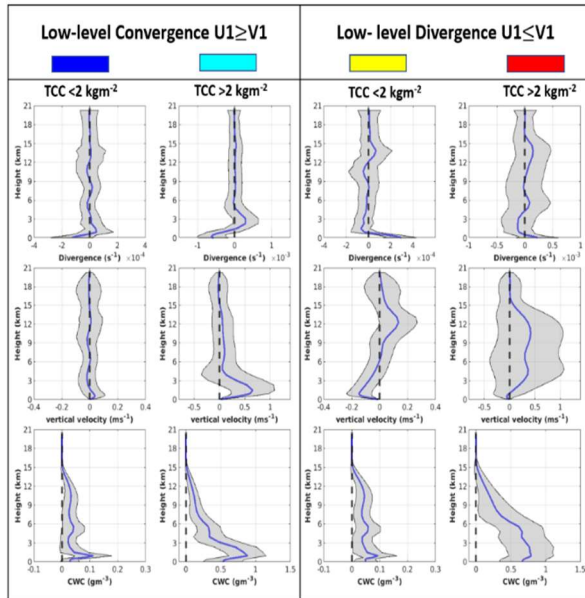


Figure 10. mean vertical profiles (blue line) and ± 1 standard deviations (shaded area) of: wind divergence (top row), vertical velocity (middle row), and condensate water content (bottom row).

(b) Experiment (S5)

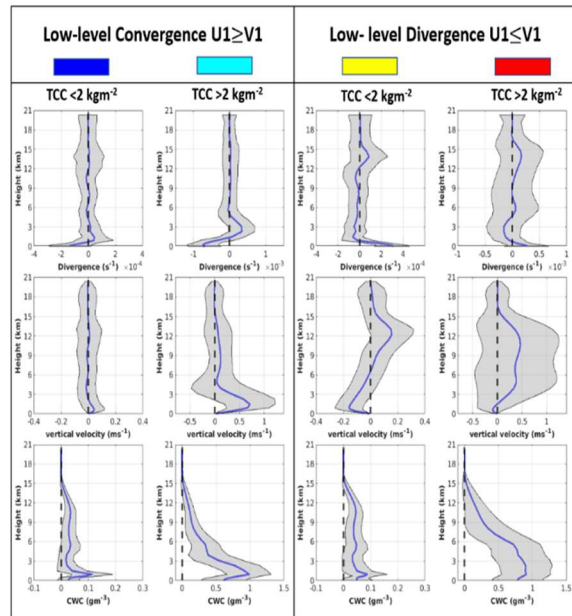


Figure 11. As in Fig. 10, except for experiment (S5).

(c) Experiment (S7)

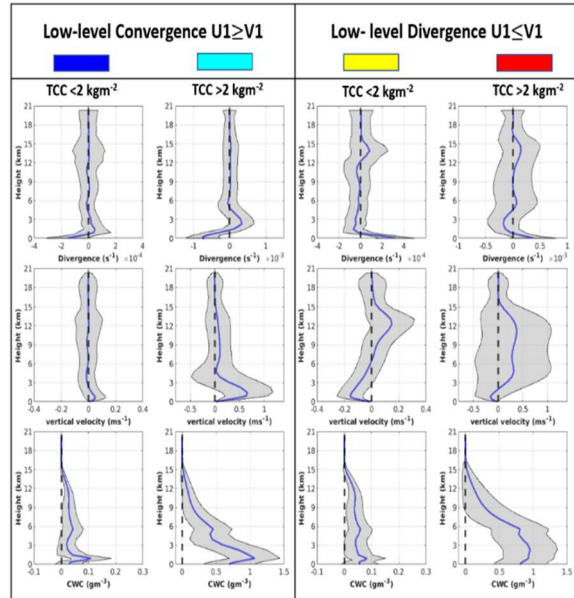


Figure 12. As in Fig. 10, except for experiment (S7).

4. RESULTS

The analysis introduces a novel technique that delineates four types of vertical structures for precipitating regions, through the correlation of deep layers of updrafts with near-surface divergence and total condensate precipitation. This method results in a classification of four well-recognized convective precipitation structures— anvil regions, shallow convection, stratiform precipitation, and deep convection as illustrated in Figure 8. The classification performs consistently across the three simulations of Hurricane Rita's structure, intensity, and evolution. Armed with this new understanding of the physical interpretation of the geophysical structure of the four regions in this study, we embarked on trying to understand the role that the amount (fraction) of each convection, and its spatial distribution, play in the evolution of storms. Motivated by this, we investigate how the structure of the four convective groups changes over time with respect to the center of the storm. Fig. 13 examined the fraction that each of the four regions occupies into 50-km annuli bins from the storm center to 250 km as a function of time for experiment (S2). Key phases in the storm's evolution are highlighted with vertical dashed lines for reference. Our findings reveal significantly more precipitation is observed in the inner region compared to the outer region and the model-simulated TC intensifies when significant deep convection develops near the storm center and weakens when deep convection occurs farther away just before the onset of decay. These findings are consistent with observational studies of Black et al. (1996) and Jorgensen, et al. (1985).

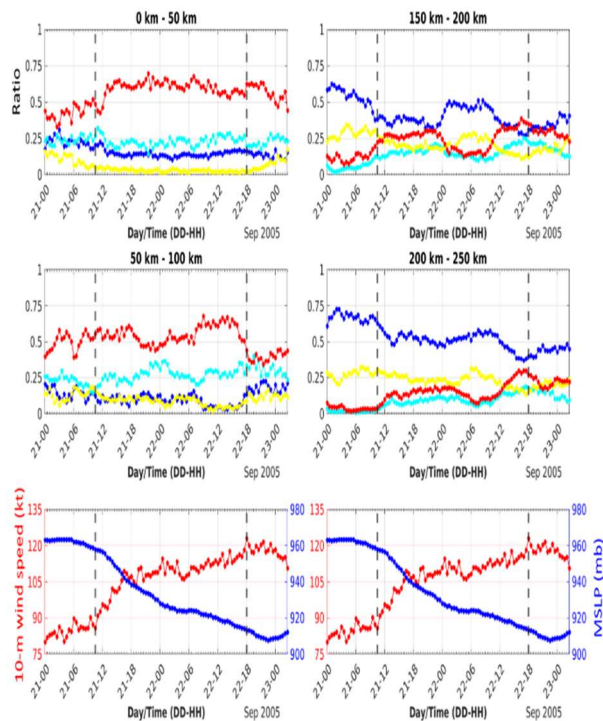


Figure 13. Evolution of the fractions of the different precipitating regions over a couple of the important regions – the inner region (0-50 km and 50-100 km) on the left and the outer region (150-200 km and 200-250 km) on the right. The evolution of the hurricane is represented by the graphs on the bottom of each column that show the evolution of the wind speed (in red) and that of the minimum surface pressure (in blue). Important phases of evolution are marked with two vertical dashed lines (in black). The first line shows the onset of Rapid Intensification (RI) and the second one marks a time just before the onset of decay.

5. FUTURE WORK

Our next steps will extend our previous work in several directions. (1) We will use model simulations of convective storms, including hurricanes and mesoscale convective systems (MCSs), with the goal to understand the relationship between the evolution of the convergence and that of the precipitation for a more rigorous verification of our proxy-detector for deep convection. (2) Study this relationship of deep convection to the storm structure and intensity. (3) We will investigate the importance of the shear vector (magnitude and direction) on deep convection development. (4) Apply the model-established relationships to satellite retrievals to understand whether the detection of deep convection is working.

REFERENCES

Black, M. L., Burpee, R. W. & Marks Jr., F. D., 1996. Vertical motion characteristics of tropical cyclones

determined with airborne Doppler radial velocities. *J. Atmos. Sci.*, Volume 53, p. 1887–1909.

Braun, S. A., 2006. High-Resolution Simulation of Hurricane Bonnie (1998). Part II: Water Budget. *J. Atmos. Sci.*, Volume 63, pp. 43–64, <https://doi.org/10.1175/JAS3609.1>.

Dai, N. et al., 2022. Observed Links between Deep Convection Aggregation and Tropical Cloud Variations. 35th Conference on Climate Variability and Change, 102nd AMS Annual Meeting.

DeMaria, M. & Kaplan, J., 1994a. Sea surface temperature and the maximum intensity of Atlantic tropical cyclones. *J. Climate*, Volume 7, pp. 1324–1334, [https://doi.org/10.1175/1520-0442\(1994\)007<1324:SSTATM>2.0.CO;2](https://doi.org/10.1175/1520-0442(1994)007<1324:SSTATM>2.0.CO;2).

Gray, W. M., 1968. Global view of the origin of tropical disturbances and storms. *Mon. Wea. Rev.*, Volume 96, pp. 669–700, [https://doi.org/10.1175/1520-0493\(1968\)096<0669:GVOTOO>2.0.CO;2](https://doi.org/10.1175/1520-0493(1968)096<0669:GVOTOO>2.0.CO;2).

Guimond, S. R., Heymsfield, G. M. & Turk, F. J., 2010. Multiscale observations of Hurricane Dennis (2005): The effects of hot towers on rapid intensification. *J. Atmos. Sci.*, Volume 67, pp. 633–654, [doi:10.1175/2009JAS3119.1](https://doi.org/10.1175/2009JAS3119.1).

Hazelton, A. T., Rogers, R. & Hart, R. E., 2015. Shear-relative asymmetries in tropical cyclone eyewall slope. *Mon. Wea. Rev.*, Volume 143, pp. 883–903, [doi:10.1175/MWR-D-14-00122.1](https://doi.org/10.1175/MWR-D-14-00122.1).

Hendricks, E. A., Montgomery, M. T. & Davis, C. A., 2004. The role of “vortical” hot towers in the formation of Tropical Cyclone Diana (1984). *J. Atmos. Sci.*, Volume 61, pp. 1209–1232, [doi:10.1175/1520-0469\(2004\)061<1209:TROVHT>2.0.CO;2](https://doi.org/10.1175/1520-0469(2004)061<1209:TROVHT>2.0.CO;2).

Holbach, H. M. & Bourassa, M. A., 2014. The Effects of Gap-Wind-Induced Vorticity, the Monsoon Trough, and the ITCZ on East Pacific Tropical Cyclogenesis. *Mon. Wea. Rev.*, Volume 142, pp. 1312–1325, <https://doi.org/10.1175/MWR-D-13-00218.1>.

Hotelling, H., 1992. Relations between two sets of variates. In *Breakthroughs in statistics: methodology and distribution*. Springer New York, pp. 162-190.

Hristova-Veleva, S. et al., 2021. Impact of Microphysical Parameterizations on Simulated Hurricanes—Using Multi-Parameter Satellite Data to Determine the Particle Size Distributions that Produce Most Realistic Storms. *Atmosphere* 12, p. 154. <https://doi.org/10.3390/atmos120201542>.

Jiang, H., 2012. The relationship between tropical cyclone intensity change and the strength of inner-core

- convection. *Mon. Wea. Rev.*, Volume 140, pp. 1164–1176, doi:10.1175/MWR-D-11-00134.1.
- Jorgensen, D. P., Zipser, E. J. & LeMone, M. A., 1985. Vertical motions in intense hurricanes. *J. Atmos. Sci.*, Volume 42, p. 839–856.
- Kaplan, J. & DeMaria, M., 2003. Large-scale characteristics of rapidly intensifying tropical cyclones in the North Atlantic basin. *Wea. Forecasting*, Volume 18, pp. 1093–1108, [https://doi.org/10.1175/1520-0434\(2003\)018<1093:LCORIT>2.0.CO;2](https://doi.org/10.1175/1520-0434(2003)018<1093:LCORIT>2.0.CO;2).
- Kelley, O. A., Stout, J. & Halverson, J. B., 2004. Tall precipitation cells in tropical cyclone eyewalls are associated with tropical cyclone intensification. *Geophys. Res. Lett.*, Volume 31, pp. L24112, doi:10.1029/2004GL021616.
- Kieper, M. E. & Jiang, H., 2012. Predicting tropical cyclone rapid intensification using the 37 GHz ring pattern identified from passive microwave measurements. *Geophys. Res. Lett.*, Volume 39, pp. L13804, doi:10.1029/2012GL052115.
- King, G. P., Portabella, M., Lin, W. & Stoffelen, A., 2022. Correlating Extremes in Wind Divergence with Extremes in Rain over the Tropical Atlantic. *Remote Sens.*, Volume 14, p. 1147. <https://doi.org/10.3390/rs14051147>.
- Klemp, J. B., 2006. Advances in the WRF model for convection-resolving forecasting. *Adv. Geosci.*, Volume 7, pp. 25–29, <https://doi.org/10.5194/adgeo-7-25-2006>.
- Leighton, H. et al., 2018. Azimuthal Distribution of Deep Convection, Environmental Factors, and Tropical Cyclone Rapid Intensification: A Perspective from HWRF Ensemble Forecasts of HuA Perspective from HWRF Ensemble Forecasts of Hurricane Edouard (2014). *J. Atmos. Sci.*, Volume 75, pp. 275–295, <https://doi.org/10.1175/JAS-D-17-0171.1>.
- Liu, C.-Y. et al., 2022. Characteristics of deep convective clouds, precipitation, and cloud properties of rapidly intensifying tropical cyclones in the western North Pacific. *Journal of Geophysical Research*, Volume 127, p. e2022JD037328. <https://doi.org/10.1029/2022JD037328>.
- Merrill, R. T., 1988. Environmental influences on hurricane intensification. *J. Atmos. Sci.*, Volume 45, pp. 1678–1687, [https://doi.org/10.1175/1520-0469\(1988\)045<1678:EIOHI>2.0.CO;2](https://doi.org/10.1175/1520-0469(1988)045<1678:EIOHI>2.0.CO;2).
- Miyamoto, Y. & Takemi, T., 2015. A triggering mechanism for rapid intensification of tropical cyclones. *J. Atmos. Sci.*, Volume 72, pp. 2666–2681, doi:10.1175/JAS-D-14-0193.1.
- Montgomery, M. T., Nicholls, M. E., Cram, T. A. & Saunders, A. B., 2006. A “vortical” hot tower route to tropical cyclogenesis. *J. Atmos. Sci.*, Volume 63, pp. 355–386, doi:10.1175/JAS3604.1.
- Montgomery, M. T. & Smith, R. K., 2012. Paradigms for tropical-cyclone intensification. *Australian Meteorological and Oceanographic Journal*, Volume 64, pp. 37–66. <https://doi.org/10.1071/ES14005>.
- Montgomery, M. T., Zhang, J. A. & Smith, R. K., 2014. An analysis of the observed low-level structure of rapidly intensifying and mature Hurricane Earl (2010). *Quart. J. Roy. Meteor. Soc.*, Volume 140, pp. 2132–2146, doi:10.1002/qj.2283.
- Nolan, D. S., Moon, Y. & Stern, D. P., 2007. Tropical cyclone intensification from asymmetric convection: Energetics and efficiency. *J. Atmos. Sci.*, Volume 64, pp. 3377–3405, doi:10.1175/JAS3988.1.
- Pendergrass, A. G. & Willoughby, H. E., 2009. Diabatically induced secondary flows in tropical cyclones. Part I: Quasi-steady forcing. *Mon. Wea. Rev.*, Volume 137, pp. 805–821, doi:10.1175/2008MWR2657.1.
- Reasor, P. D., Eastin, M. D. & Gamache, J. F., 2009. Rapidly intensifying Hurricane Guillermo (1997). Part I: Low-wavenumber structure and evolution. *Mon. Wea. Rev.*, Volume 137, pp. 603–631, doi:10.1175/2008MWR2487.1.
- Rogers, R., 2010. Convective-scale structure and evolution during a high-resolution simulation of tropical cyclone rapid intensification. *J. Atmos. Sci.*, Volume 67, pp. 44–70, doi:10.1175/2009JAS3122.1.
- Rogers, R. F., Reasor, P. D. & Zhang, J. A., 2015. Multiscale structure and evolution of Hurricane Earl (2010) during rapid intensification. *Mon. Wea. Rev.*, Volume 143, pp. 536–562, doi:10.1175/MWR-D-14-00175.1.
- Rogers, R., Reasor, P. & Lorsolo, S., 2013. Airborne Doppler observations of the inner-core structural differences between intensifying and steady-state tropical cyclones. *Mon. Wea. Rev.*, Volume 141, pp. 2970–2991, doi:10.1175/MWR-D-12-00357.1.
- Sanger, N. T., Montgomery, M. T., Smith, R. K. & Bell, M. M., 2014. An observational study of tropical cyclone spinup in Supertyphoon Jangmi (2008) from 24 to 27 September. *Mon. Wea. Rev.*, Volume 142, pp. 3–28, doi:10.1175/MWR-D-12-00306.1.
- Schubert, W. H. & Hack, J. J., 1982. Inertial stability and tropical cyclone development. *J. Atmos. Sci.*, Volume 39, pp. 1687–1697, doi:10.1175/1520-0469(1982)039<1687:ISATCD>2.0.CO;2.
- Shapiro, L. J. & Willoughby, H. E., 1982. The response of balanced hurricanes to local sources of heat and momentum. *J. Atmos. Sci.*, Volume 39, pp. 378–394,

doi:10.1175/1520-0469(1982)039<0378:TROBHT>2.0.CO;2.

Smith, R. K., Montgomery, M. T. & Sang, N. V., 2009. Tropical cyclone spin up revisited. *Quart. J. Roy. Meteor. Soc.*, Volume 135, pp. 1321–1335, doi:10.1002/qj.428.

Stevenson, S. N., Corbosiero, K. L. & Molinari, J., 2014. The convective evolution and rapid intensification of Hurricane Earl (2010). *Mon. Wea. Rev.*, Volume 142, pp. 4364–4380, doi:10.1175/MWR-D-14-00078.1.

Susca-Lopata, G., Zawislak, J., Zipser, E. J. & Rogers, R. F., 2015. The role of observed environmental conditions and precipitation evolution in the rapid intensification of Hurricane Earl (2010). *Mon. Wea. Rev.*, Volume 143, pp. 2207–2223, doi:10.1175/MWR-D-14-00283.1.

Tao, C. & Jiang, H., 2015. Distributions of shallow to very deep precipitation–convection in rapidly intensifying tropical cyclones. *J. Climate*, Volume 28, pp. 8791–8824, doi:10.1175/JCLI-D-14-00448.1.

Vigh, J. L. & Schubert, W. H., 2009. Rapid development of the tropical cyclone warm core. *J. Atmos. Sci.*, 66. *J. Atmos. Sci.*, Volume 66, pp. 3335–3350, doi:10.1175/2009JAS3092.1.

Zagrodnik, J. P. & Jiang, H., 2014. Rainfall, convection, and latent heating distributions in rapidly intensifying tropical cyclones. *J. Atmos. Sci.*, Volume 71, pp. 2789–2809, doi:10.1175/JAS-D-13-0314.1.

Zhang, J. A. et al., 2013. Asymmetric hurricane boundary layer structure from dropsonde composites in relation to the environmental wind shear. *Mon. Wea. Rev.*, Volume 141, pp. 3968–3984, doi:10.1175/MWR-D-12-00335.1.